thymus contains IFN-α-producing CD11c$^-$, myeloid CD11c$^+$, and mature interdigitating dendritic cells. *J. Clin. Invest.* 107: 835–844.
11. Sprent, J., and S. R. Webb. 1995. Intrathymic and extrathymic clonal deletion of T cells. *Curr. Opin. Immunol.* 7: 196–205.
12. Heino, M., P. Peterson, N. Sillanpaa, S. Guerin, L. Wu, G. Anderson, H. S. Scott, S. E. Antonarakis, J. Kudoh, N. Shimizu, et al. 2000. RNA and protein expression of the murine *autoimmune regulator gene (Aire)* in normal, RelB-deficient and in NOD mouse. *Eur. J. Immunol.* 30: 1884–1893.
13. Kyewski, B., and J. Derbinski. 2004. Self-representation in the thymus: an extended view. *Nat. Rev. Immunol.* 4: 688–698.
14. Proietto, A. I., S. van Dommelen, P. Zhou, A. Rizzitelli, A. D'Amico, R. J. Steptoe, S. H. Naik, M. H. Lahoud, Y. Liu, P. Zheng, et al. 2008. Dendritic cells in the thymus contribute to T-regulatory cell induction. *Proc. Natl. Acad. Sci. USA* 105: 19869–19874.
15. Heinzel, K., C. Benz, and C. C. Bleul. 2007. A silent chemokine receptor regulates steady-state leukocyte homing in vivo. *Proc. Natl. Acad. Sci. USA* 104: 8421–8426.
16. Kim, C. H. 2005. The greater chemotactic network for lymphocyte trafficking: chemokines and beyond. *Curr. Opin. Hematol.* 12: 298–304.
17. Schutyser, E., A. Richmond, and J. Van Damme. 2005. Involvement of CC chemokine ligand 18 (CCL18) in normal and pathological processes. *J. Leukocyte Biol.* 78: 14–26.
18. Vecchi, A., L. Massimiliano, S. Ramponi, W. Luini, S. Bernasconi, R. Bonecchi, P. Allavena, M. Parmentier, A. Mantovani, and S. Sozzani. 1999. Differential responsiveness to constitutive vs. inducible chemokines of immature and mature mouse dendritic cells. *J. Leukocyte Biol.* 66: 489–494.
19. Niess, J. H., S. Brand, X. Gu, L. Landsman, S. Jung, B. A. McCormick, J. M. Vyas, M. Boes, H. L. Ploegh, J. G. Fox, et al. 2005. CX3CR1-mediated dendritic cell access to the intestinal lumen and bacterial clearance. *Science* 307: 254–258.
20. Gao, J. L., T. A. Wynn, Y. Chang, E. J. Lee, H. E. Broxmeyer, S. Cooper, H. L. Tiffany, H. Westphal, J. Kwon-Chung, and P. M. Murphy. 1997. Impaired host defense, hematopoiesis, granulomatous inflammation and type 1-type 2 cytokine balance in mice lacking CC chemokine receptor 1. *J. Exp. Med.* 185: 1959–1968.
21. Combadiere, C., S. Potteaux, J. L. Gao, B. Esposito, S. Casanova, E. J. Lee, P. Debre, A. Tedgui, P. M. Murphy, and Z. Mallat. 2003. Decreased atherosclerotic lesion formation in CX3CR1/apolipoprotein E double knockout mice. *Circulation* 107: 1009–1016.
22. Murai, M., H. Yoneyama, T. Ezaki, M. Suematsu, Y. Terashima, A. Harada, H. Hamada, H. Asakura, H. Ishikawa, and K. Matsushima. 2003. Peyer's patch is the essential site in initiating murine acute and lethal graft-versus-host reaction. *Nat. Immunol.* 4: 154–160.
23. Kuziel, W. A., S. J. Morgan, T. C. Dawson, S. Griffin, O. Smithies, K. Ley, and N. Maeda. 1997. Severe reduction in leukocyte adhesion and monocyte extravasation in mice deficient in CC chemokine receptor 2. *Proc. Natl. Acad. Sci. USA* 94: 12053–12058.
24. Brewer, J. A., O. Kanagawa, B. P. Sleckman, and L. J. Muglia. 2002. Thymocyte apoptosis induced by T cell activation is mediated by glucocorticoids in vivo. *J. Immunol.* 169: 1837–1843.
25. Mayor, S., and R. E. Pagano. 2007. Pathways of clathrin-independent endocytosis. *Nat. Rev. Mol. Cell Biol.* 8: 603–612.
26. Sandvig, K., S. Olsnes, O. W. Petersen, and B. van Deurs. 1987. Acidification of the cytosol inhibits endocytosis from coated pits. *J. Cell Biol.* 105: 679–689.
27. Zal, T., A. Volkmann, and B. Stockinger. 1994. Mechanisms of tolerance induction in major histocompatibility complex class II-restricted T cells specific for a blood-borne self-antigen. *J. Exp. Med.* 180: 2089–2099.
28. Bubanovic, I. V. 2003. Failure of blood-thymus barrier as a mechanism of tumor and trophoblast escape. *Med. Hypotheses* 60: 315–320.
29. Balazs, M., F. Martin, T. Zhou, and J. Kearney. 2002. Blood dendritic cells interact with splenic marginal zone B cells to initiate T-independent immune responses. *Immunity* 17: 341–352.
30. Murphy, P. M., M. Baggiolini, I. F. Charo, C. A. Hebert, R. Horuk, K. Matsushima, L. H. Miller, J. J. Oppenheim, and C. A. Power. 2000. International union of pharmacology: XXII. Nomenclature for chemokine receptors. *Pharmacol. Rev.* 52: 145–176.
31. Vremec, D., J. Pooley, H. Hochrein, L. Wu, and K. Shortman. 2000. CD4 and CD8 expression by dendritic cell subtypes in mouse thymus and spleen. *J. Immunol.* 164: 2978–2986.
32. Ladi, E., T. A. Schwickert, T. Chtanova, Y. Chen, P. Herzmark, X. Yin, H. Aaron, S. W. Chan, M. Lipp, B. Roysam, and E. A. Robey. 2008. Thymocyte-dendritic cell interactions near sources of CCR7 ligands in the thymic cortex. *J. Immunol.* 181: 7014–7023.
33. McCaughtry, T. M., T. A. Baldwin, M. S. Wilken, and K. A. Hogquist. 2008. Clonal deletion of thymocytes can occur in the cortex with no involvement of the medulla. *J. Exp. Med.* 205: 2575–2584.
34. Sawanobori, Y., S. Ueha, M. Kurachi, T. Shimaoka, J. E. Talmadge, J. Abe, Y. Shono, M. Kitabatake, K. Kakimi, N. Mukaida, and K. Matsushima. 2008. Chemokine-mediated rapid turnover of myeloid-derived suppressor cells in tumor-bearing mice. *Blood* 111: 5457–5466.
35. Tsou, C. L., W. Peters, Y. Si, S. Slaymaker, A. M. Aslanian, S. P. Weisberg, M. Mack, and I. F. Charo. 2007. Critical roles for CCR2 and MCP-3 in monocyte mobilization from bone marrow and recruitment to inflammatory sites. *J. Clin. Invest.* 117: 902–909.
36. Mori, K., M. Itoi, N. Tsukamoto, H. Kubo, and T. Amagai. 2007. The perivascular space as a path of hematopoietic progenitor cells and mature T cells between the blood circulation and the thymic parenchyma. *Int. Immunol.* 19: 745–753.
37. Haribhai, D., D. Engle, M. Meyer, D. Donermeyer, J. M. White, and C. B. Williams. 2003. A threshold for central T cell tolerance to an inducible serum protein. *J. Immunol.* 170: 3007–3014.
38. Quinones, M. P., S. K. Ahuja, F. Jimenez, J. Schaefer, E. Garavito, A. Rao, G. Chenaux, R. L. Reddick, W. A. Kuziel, and S. S. Ahuja. 2004. Experimental arthritis in CC chemokine receptor 2-null mice closely mimics severe human rheumatoid arthritis. *J. Clin. Invest.* 113: 856–866.
39. Lauritzsen, G. F., P. O. Hofgaard, K. Schenck, and B. Bogen. 1998. Clonal deletion of thymocytes as a tumor escape mechanism. *Int. J. Cancer* 78: 216–222.
40. Paessens, L. C., D. M. Fluitsma, and Y. van Kooyk. 2008. Haematopoietic antigen-presenting cells in the human thymic cortex: evidence for a role in selection and removal of apoptotic thymocytes. *J. Pathol.* 214: 96–103.

Liver Fibrosis in Patients with Chronic Hepatitis C: Noninvasive Diagnosis by Means of Real-time Tissue Elastography—Establishment of the Method for Measurement[1]

Yohei Koizumi, MD
Masashi Hirooka, MD, PhD
Yoshiyasu Kisaka, MD, PhD
Ichiro Konishi, MD, PhD
Masanori Abe, MD, PhD
Hidehiro Murakami, MD, PhD
Bunzo Matsuura, MD, PhD
Yoichi Hiasa, MD, PhD
Morikazu Onji, MD, PhD

Purpose: To prospectively measure liver stiffness with real-time tissue elastography in patients with chronic hepatitis C and to compare the results with those of clinical assessment of fibrosis by using histologic stage as the reference standard.

Materials and Methods: All subjects gave informed consent, and the study was approved by the institutional ethics committee. Seventy hospitalized patients (46 men, 24 women; mean age, 65.5 years ± 11.7 [standard deviation]; age range, 33–87 years) with chronic hepatitis C underwent real-time elastography between January 2009 and September 2009. Elastography was performed at four liver locations by two independent observers. The elastic ratio (ratio of the value in the intrahepatic venous small vessels divided by the value in the hepatic parenchyma) was calculated and was compared with histologic fibrosis stage at liver biopsy. The elastic ratio and clinical fibrosis markers were assessed by using receiver operating characteristic (ROC) analysis. The differences between body site and observers were assessed with κ statistics and intraclass correlation coefficients (ICCs).

Results: Real-time tissue elastography cutoff values were 2.73 for F of 2 or greater, 3.25 for F of 3 or greater, and 3.93 for F of 4. No site differences were observed (κ = 0.835, ICC = 0.966), and the elastic ratio measurement was correlated between the two examiners (r^2 = 0.869, $P < .0001$). The areas under the ROC curves for elastic ratio, hyaluronic acid, type IV collagen, aspartate aminotransferase–to–platelet ratio index, FibroIndex, Forns score, and Hepascore were 0.95, 0.32, 0.73, 0.76, 0.76, 0.87, and 0.70, respectively; the elastic ratio performed better than the serum fibrosis markers and other scores.

Conclusion: Real-time tissue elastography is not invasive and could be used to evaluate liver fibrosis in patients with chronic hepatitis C.

Supplemental material: *http://radiology.rsna.org/lookup/suppl/doi:10.1148/radiol.10100319/-/DC1*

[1] From the Department of Gastroenterology and Metabology, Ehime University Graduate School of Medicine, Shitsukawa, Toon, Ehime 791-0295, Japan. Received February 9, 2010; revision requested March 24; revision received June 22; accepted July 13; final version accepted August 11. Supported by a Grant-in-Aid for Scientific Research (C) (Japan Society for the Promotion of Science, KAKENHI 21590848) and the Program for Enhancing Systematic Education in Graduate School from the Ministry of Education, Culture, Sports, Science and Technology, Tokyo, Japan.
Address correspondence to Y.H. (e-mail: *hiasa@m.ehime-u.ac.jp*).

Chronic viral hepatitis infection increases liver fibrosis and stiffness and is an important cause of liver cirrhosis (1). Although liver biopsy is the reference standard for the diagnosis of liver fibrosis (2), it is an invasive procedure, which is difficult to perform in patients who need to be examined repeatedly to monitor the progression of liver fibrosis. Moreover, the evaluation of fibrosis with liver biopsy is associated with adverse events (3), sampling errors (4,5), and interpathologist and intrapathologist variabilities (6). Therefore, many studies have evaluated other noninvasive methods, such as the use of sonographic transient elastography (FibroScan; EchoSens, London, England) (7) and acoustic radiation force impulse (8) and laboratory tests, such as the aspartate aminotransferase–to–platelet ratio index, the FibroIndex, the Forns score, and the Hepascore, for the assessment of liver fibrosis stage.

Transient elastography is one of the techniques that can be used to evaluate mean tissue stiffness noninvasively (7). Results of several recent studies (9) have shown that measurements of liver stiffness with transient elastography are well correlated with fibrosis METAVIR stages. In addition, transient elastography is advantageous in that it can be repeatedly performed, does not require a highly experienced operator, and has a low risk of complications. However, there is a problem with reproducibility at identical measurement positions (10). In addition, it is not a real-time technique, because the image is not visible while the measurement is being taken. The reproducibility of transient elastography is also substantially reduced in patients with steatosis and increased body mass index (BMI) because the modality of ultrasonography (US) itself has limitations for visualizing the liver clearly in such patients (11).

Real-time tissue elastography is a relatively new method for the measurement of tissue elasticity. It uses a B-mode US machine, incorporating elastography into the conventional US scanner (12). In the previously reported technique, a US probe is used to slightly compress or relax the body (13), and the echo signals are captured in real time. This device calculates the relative hardness of tissue and displays this information as real-time color images (14); it can display tissue elasticity images and conventional B-mode images at the same time.

The purpose of this prospective study was to measure liver stiffness with real-time elastography in patients with chronic hepatitis C and to compare the results with those of other clinical assessments of fibrosis by using the histologic stage of fibrosis as the reference standard.

Advances in Knowledge

- In patients with hepatitis C, the areas under the receiver operating characteristic curves for prediction of fibrosis by means of elastic ratio, hyaluronic acid level, type IV collagen level, aspartate aminotransferase–to–platelet ratio index, FibroIndex, Forns score, and Hepascore were 0.95, 0.32, 0.73, 0.76, 0.76, 0.87, and 0.70, respectively, indicating that the elastic ratio performed better than the other serum fibrosis markers and scores.
- For METAVIR stages identified at histologic examination, real-time elastography cutoff values were 2.73 for F of 2 or greater, 3.25 for F of 3 or greater, and 3.93 for F of 4.
- Our results were independent of observer ($r^2 = 0.869$, $P < .0001$) and measurement positioning site (intraclass correlation coefficient: 0.966, $\kappa = 0.835$).

Implications for Patient Care

- Real-time elastography is not invasive and could be used to repeatedly evaluate liver fibrosis.
- Real-time elastography could be a powerful tool for time-course evaluation of liver cirrhosis during antiviral therapy.

Materials and Methods

Patients

The study protocol was approved by the institutional review board, and written informed consent was obtained. All enrolled patients underwent liver biopsy as part of the study. Seventy patients with chronic hepatitis C (mean age, 65.5 years ± 11.7 [standard deviation]; range, 33–87 years) were hospitalized in the Department of Gastroenterology and Metabology, Ehime University Hospital, Japan, from January 2009 to September 2009, and liver stiffness, which is related to the grade of liver fibrosis, was measured. Of the 70 patients, 46 were men (mean age, 63.5 years ± 13.9; range, 33–87 years), and 24 were women (mean age, 66.6 years ± 10.3; range, 46–84 years).

Inclusion criteria were the presence of hepatitis C virus (HCV) ribonucleic acid in serum according to real-time polymerase chain reaction and positive HCV antibody. The exclusion criteria were ascites (because that might interfere with measurements), coinfection with other viruses such as hepatitis B virus, other liver diseases such as primary biliary

Published online
10.1148/radiol.10100319

Radiology 2011; 258:610–617

Abbreviations:
AUC = area under the ROC curve
BMI = body mass index
CI = confidence interval
ICC = intraclass correlation coefficient
ROC = receiver operating characteristic
ROI = region of interest

Author contributions:
Guarantors of integrity of entire study, Y. Koizumi, M.H., Y. Kisaka, I.K., M.A., B.M., Y.H., M.O.; study concepts/study design or data acquisition or data analysis/interpretation, all authors; manuscript drafting or manuscript revision for important intellectual content, all authors; manuscript final version approval, all authors; literature research, Y. Koizumi, M.H., Y. Kisaka, I.K., M.A., B.M., Y.H.; clinical studies, Y. Koizumi, M.H., Y. Kisaka, I.K., M.A., H.M., B.M., Y.H.; experimental studies, Y. Koizumi, M.H., Y. Kisaka, I.K., M.A., Y.H.; statistical analysis, Y. Koizumi, M.H., Y. Kisaka, I.K., M.A., Y.H.; and manuscript editing, Y. Koizumi, M.H., Y. Kisaka, I.K., M.A., B.M., Y.H., M.O.

Authors stated no financial relationship to disclose.

Figure 1

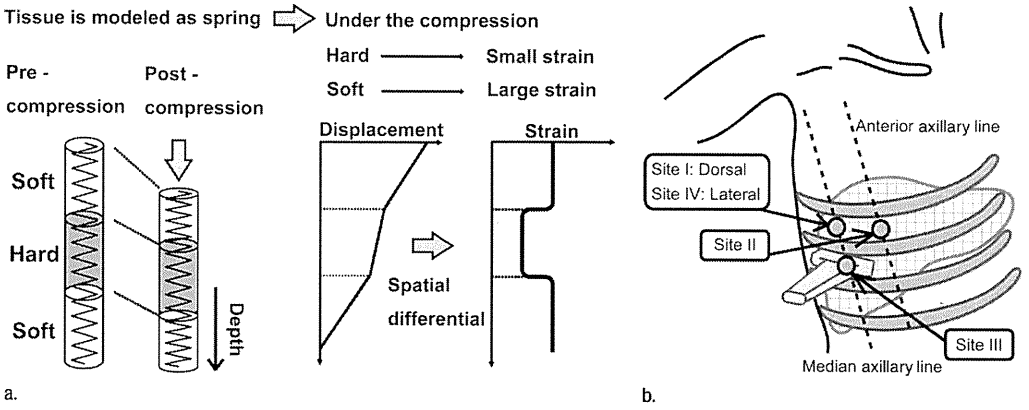

Figure 1: **(a)** The underlying method of real-time tissue elastography is the measurement and imaging of the strain distribution by adding the static pressure from the body surface; this is illustrated as a spring model. **(b)** The four measurement sites for real-time tissue elastography.

cirrhosis, and excessive alcohol consumption. (So that we could compare the METAVIR stages, which grade liver fibrosis only in patients with hepatitis C).

BMI and skin fold thickness were measured to determine whether they had any effects on real-time tissue elastography measurements.

Method for Measurement of Liver Stiffness

The underlining principle of real-time tissue elastography is illustrated in Figure 1a by using a spring model. When a spring is compressed, displacement in each section of the spring depends on the stiffness of the spring: A soft spring compresses more than a hard spring. The strain distribution, and in turn the stiffness in the spring, is measured by spatially differentiating the displacement at each location. On the basis of a previous report (13), we believed that compressing and relaxing the tissue with the US probe would be needed to measure the stiffness. However, we determined that we could measure the liver stiffness without adding any pressure from the probe because the liver itself receives pressure from the heartbeat automatically. Reflected US echoes are then used to compute the displacement and, thus, the strain distribution in the tissue. The examiners measured liver stiffness at four sites (Fig 1b), using the same positioning sites of the body as Boursier et al (10). The measurement sites were defined as follows: Site I was the dorsal decubitus and on the median axillary line and the first intercostal space; site II, the dorsal decubitus and on the anterior axillary line and the first intercostal space; site III, the dorsal decubitus and on the median axillary line and the second intercostal space; and site IV, the lateral decubitus and on the median axillary line and the first intercostal space. Real-time tissue elastography was performed five times at four measurement sites by two observers for each patient, in exhalation or inspiration to ensure that the liver was adequately depicted. The mean of the five measurements was calculated for comparison with histologic results.

Elastic Ratio

Hepatic elasticity was measured by using a US scanner with real-time tissue elastography (EUB-7500; Hitachi Medical Systems, Tokyo, Japan). We used a linear probe (EUP-L52; central frequency, 5.5 MHz). This scanner displays the color-coded elastography image overlaid on the B-mode image in real time (Fig 2a). Because this displayed color-coded elastography image shows only the relative tissue stiffness, a quantitative measuring technique called the elastic ratio was utilized.

The elastic ratio is the ratio of strain distribution in two selected regions of interest (ROIs). First, it was important to identify whether the hepatic vein or the portal vein would be a better internal control. We measured the value in the hepatic vein and portal vein for all 70 enrolled patients. The ROC curves of the elastic ratio calculated by using the ROI of the hepatic vein and the ROI of the portal vein as internal controls are shown in Figure 2b. The areas under the ROC curves (AUCs) of the elastic ratios obtained by using the hepatic vein as an internal control were higher than those obtained by using the portal vein as an internal control (intraclass correlation coefficient [ICC]: 0.953 [95% confidence interval {CI}: 0.903, 0.998] vs 0.731 [95% CI: 0.649, 0.886]; $P = .0006$). On the basis of the AUCs, the hepatic veins were used as an internal control. The ROI was placed on intrahepatic venous small vessels with a diameter of less than 3 mm and the hepatic parenchyma simultaneously. Subsequently, the ratio of the value in the intrahepatic venous small vessels was divided by the value in the hepatic parenchyma to generate the elastic ratio.

The elasticity of the hepatic vein was used as the reference because the elasticity of the veins does not change over time, since they do not undergo

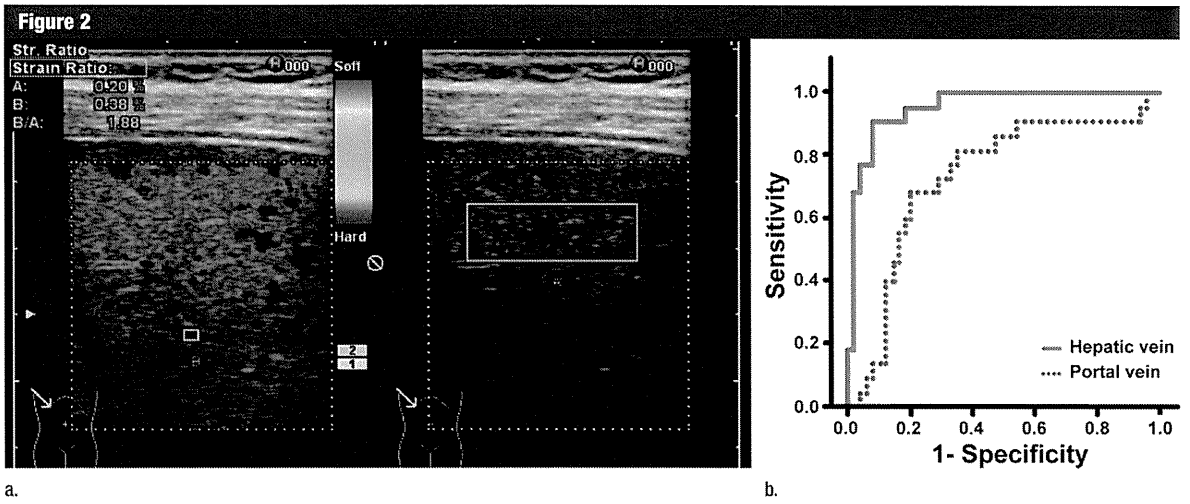

Figure 2: **(a)** The elastic ratio is measured between the tissue compressibility of the liver (right) and that of the intrahepatic small vessel (left). Red indicates that tissue is soft, and blue indicates that it is hard. Information about displacement becomes the basis of the elastic information and is obtained by using a supersonic wave signal. **(b)** Receiver operating characteristic (ROC) curves of the elastic ratio obtained by using the hepatic vein or portal vein as an internal control.

transformations with disease, such as arteriosclerosis, and it also does not increase or decrease even when liver parenchyma becomes stiffer. Thus, small vessels with a diameter of 3 mm in the liver were used as the standard for computing the elasticity ratio, and the ROI was set as large as possible (usually 0.3 × 0.5 cm). The ROI in the liver parenchyma was placed 1 cm from the liver surface and was 2 × 1 cm in size. A higher elastic ratio indicates harder hepatic elasticity, corresponding to a higher stage of fibrosis. None of the patients had liver tumors in the measurement site that might have interfered with the real-time tissue elastography.

Observers

Two hepatologists (M.H. and Y. Koizumi, with 13 and 6 years of experience, respectively) performed the liver stiffness evaluation with real-time tissue elastography; each had already performed at least 100 liver stiffness evaluations (M.H., 350; Y. Koizumi, 120) prior to the beginning of the study. Each observer measured the elastic ratio five times at four sites (Fig 1b). The second observer was blinded to the results of the first observer. Measurement time for each measurement site (time from the beginning of measurement until completion to identify the elastic ratio with five measurements after placing the ROI) was recorded for each observer. For measurement site IV, the measurement time included the time for movement of the patient.

Liver Histologic Assessment

US-guided percutaneous liver biopsy (1.6-mm-diameter and 150-mm-long needle, suction technique) was performed within 1 week after hospitalization. Liver biopsy samples less than 12 mm long were excluded, because a sampling error for identifying liver fibrosis may occur with such samples (4). Liver biopsy samples were fixed in formalin and embedded in paraffin. Slices (4 μm thick) were stained with hematoxylin-eosin and impregnated with silver. Liver biopsies that contained fewer than five portal tracts (except for cirrhosis) were excluded from the histologic analysis. Fibrosis was staged by two pathologists (one of whom was I.K., with 16 years of experience), who were blinded to all patient characteristics. Fibrosis was staged on a four-point scale according to METAVIR (F0 indicated no fibrosis; F1, portal fibrosis without septa; F2, portal fibrosis and few septa; F3, numerous septa without cirrhosis; F4, cirrhosis) (15). Activity was graded according to METAVIR as A0, none; A1, mild; A2, moderate; and A3, severe (16). Lipid share was defined as mild, 0%–30%; moderate, 30%–60%; and severe, more than 60%.

Serum Fibrosis Markers

Levels of the following blood parameters were determined: aspartate aminotransferase, alanine aminotransferase, total bilirubin, platelets, gamma-glutamyl transferase, cholesterol, urea, hyaluronic acid, type IV collagen, cholinesterase, α1 and α2 globulins, β globulins, γ-globulins, prothrombin index, apolipoprotein-A1, haptoglobin, and ferritin. The aspartate aminotransferase (AST)–to–platelet ratio index (17) was calculated as follows: (AST/UNL · 100)/platelet count. (UNL is the upper limit of the normal aspartate aminotransferase.) The FibroIndex (18) was calculated as 1.738 − 0.064 (platelet count) + 0.005 (AST) + 0.463 (gamma-globulin). Forns score (19) was calculated as 7.811 − 3.131 ln(platelet count) + 0.781 ln(gamma-glutamyl transferase) + 3.467 ln(age) − 0.014 (cholesterol). Hepascore (20) was calculated as $y/(1 + y)$, $y = \exp[-4.185818 - (0.0249 \cdot \text{age}) + 0.7464 \cdot \text{sex}] + (1.0039 \cdot \alpha2\text{-macroglobulin}) + (0.0302 \cdot \text{hyaluronic acid}) + (0.0691 \cdot \text{bilirubin}) - (0.0012 \cdot \text{gamma-glutamyl transferase})$.

Statistical Analysis

The AUC of the elastic ratio was then compared with that derived from standard laboratory tests published in the literature, including the aspartate aminotransferase–to–platelet ratio index, FibroIndex, Forns score, and Hepascore (17–20). The ROC curve was prepared by using a statistical software package (JMP, version 8; SAS Institute Japan, Tokyo, Japan).

The diagnostic performance of liver stiffness evaluation and fibrosis was determined in terms of sensitivity, specificity, positive predictive value, negative predictive value, diagnostic accuracy, and AUC. The optimal cutoff values for liver stiffness were chosen to maximize the sum of sensitivity and specificity, and positive and negative predictive values were computed for those cutoff values.

Stiffness measurements were not normally distributed. Therefore, the elastic ratio was compared with the categories of the consensus fibrosis stage by using the Kruskal-Wallis nonparametric analysis of variance test. Correlations between the elastic ratio and the histologic fibrosis stage were also analyzed by using Spearman correlation coefficients.

The correlations between the values of each observer's real-time tissue elastography measurements, as well as the site differences, were evaluated by calculating κ coefficients and ICCs. The κ coefficient was defined as follows: poor, $\kappa < 0.4$; fair to good, $0.4 \leq \kappa < 0.75$; and excellent, $0.75 \leq \kappa$ (21). The ICC was defined as follows: slight, $0 \leq$ ICC < 0.20; fair, $0.21 \leq$ ICC < 0.40; moderate, $0.41 \leq$ ICC < 0.60; substantial, $0.61 \leq$ ICC < 0.80; and almost perfect, ICC > 0.81 (22).

The estimated sample sizes according to the two-sample Student *t* test in the F1–F3 group and F4 groups were 20 and 20 respectively, given a type I error of .05, a type II error of .2, and an effect size of 1.785. Multivariate stepwise logistic regression models were used to identify independent significant factors among serum fibrosis markers, METAVIR fibrosis stage, and activity grade, steatosis, BMI, and skin fold thickness for the elastic ratio determined with real-time tissue elastography. The statistical analyses were performed by using the JMP statistical software.

Table 1

Patient Characteristics

Characteristic*	All Patients ($n = 70$)	Men ($n = 46$)	Women ($n = 24$)
Age (y)	65.5 ± 11.7	66.6 ± 10.3	63.4 ± 13.9
BMI (kg/m²)	23.2 ± 3.37	22.8 ± 3.05	23.9 ± 3.82
ALT level (IU/L)	42.8 ± 31.4	46.3 ± 35.0	35.9 ± 21.9
Serum albumin level (g/dL)	3.68 ± 0.60	3.61 ± 0.61	3.81 ± 0.57
Platelet count ($10^4/\mu L$)	14.1 ± 7.12	14.1 ± 7.68	14.1 ± 6.05
Prothrombin time (%)	91.6 ± 18.1	89.3 ± 17.7	95.9 ± 18.4
Total bilirubin (mg/dL)	0.9 ± 0.44	0.95 ± 0.49	0.77 ± 0.30
GGT level (IU/L)	55.5 ± 46.8	62.6 ± 48.1	41.9 ± 41.6
Child-Pugh class			
A	63	40	23
B	7	6	1
C	0	0	0
Histologic fibrosis stage			
F1	12	6	6
F2	16	10	6
F3	19	12	7
F4	23	18	5
Histologic activity grade			
A0	1	1	0
A1	67	44	23
A2	2	1	1
A3	0	0	0
Histologic steatosis			
Mild	68	46	22
Moderate	2	0	2
Severe	0	0	0

Note.—Data are means ± standard deviations or numbers of patients.

* ALT = alanine aminotransferase, GGT = gamma-glutamyl transferase.

Results

Patients

Between January 2009 and September 2009, 70 patients met the inclusion criteria (Table 1). There were no significant differences in age ($P = .54$) or BMI ($P = .31$) between men and women. Gamma-glutamyl transferase was significantly higher in men ($P = .02$), but no significant difference was seen in the other biochemical tests between men and women (Table 1).

The rates of interobserver agreement in determining each fibrosis stage at each site were: site I, 81.4% (57 of 70 patients); site II, 71.4% (50 of 70 patients); site III, 74.3% (52 of 70 patients); and site IV, 75.7% (53 of 70 patients). For F4 or non-F4, the rate of interobserver agreement was: site I, 97.1% (68 of 70 patients); site II, 88.6% (62 of 70 patients); site III, 88.6% (62 of 70 patients); and site IV, 92.9% (65 of 70 patients). The mean κ value for F4 or non-F4 according to the elastic ratio was excellent at each site (site I, $\kappa = 0.94 \pm 0.04$ [standard error of the mean]; site II, $\kappa = 0.77 \pm 0.075$; site III, $\kappa = 0.77 \pm 0.08$; and site IV, $\kappa = 0.85 \pm 0.06$) (Table 2). At sites I–IV, the κ value, ICCs and 95% CIs indicated that the interobserver agreement was almost the same. The time for measurement was within 5 minutes for each measurement site, and the total measurement time for four sites was not significantly different between the two examiners ($P = .93$).

Table 2

Influence of Measurement Site on Interobserver Agreement

Parameter	Measurement Site				
	I	II	III	IV	All
ICC	0.95	0.92	0.91	0.94	0.97
95% CI	0.92, 0.97	0.87, 0.95	0.83, 0.93	0.90, 0.96	0.95, 0.98
Diagnosis of F1–F4 fibrosis (κ)	0.73	0.60	0.57	0.66	0.64
Diagnosis of F4 or non-F4 fibrosis (κ)	0.94	0.77	0.77	0.86	0.84
Measurement time for M.H. (min)	2.78 ± 1.38	2.92 ± 1.31	2.78 ± 1.38	3.12 ± 1.47	11.7 ± 1.66
Measurement time for Y. Koizumi (min)	2.82 ± 1.41	2.95 ± 1.29	2.77 ± 1.35	3.23 ± 1.41	11.9 ± 1.83

Figure 3

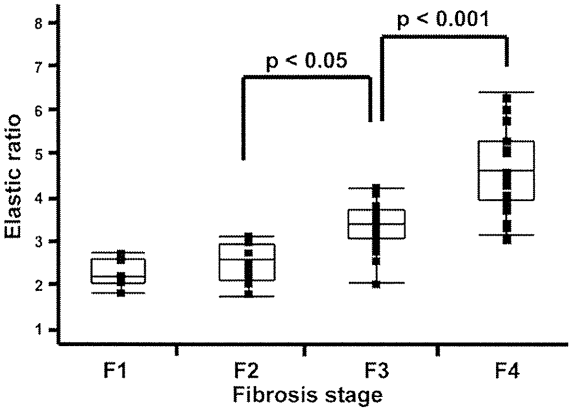

Figure 3: Graph shows elastic ratio for each fibrosis stage. The vertical axis is logarithmic scale. Tops and bottoms of the boxes = 1st and 3rd quartiles. The length of the box thus represents the interquartile range within which 50% of the values are located.

Figure 4

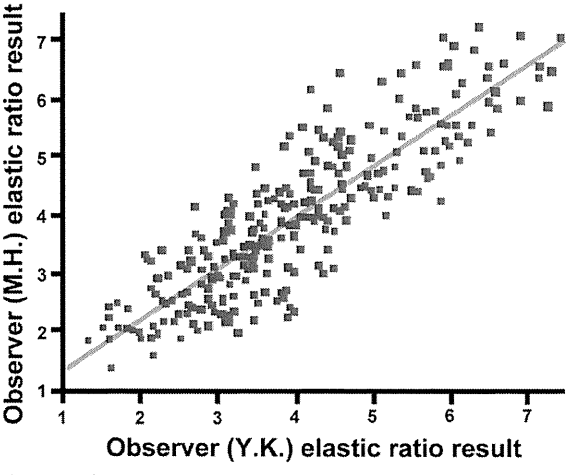

Figure 4: Graph shows correlation of elastic ratio measurement results between two examiners (Y. Koizumi and M.H., $r^2 = 0.869$, $P < .0001$).

Relationship between Liver Elastic Ratio and Histologic Parameters

The median value (95% CI) of the liver elastic ratio compared with the METAVIR fibrosis stage is shown in Figure 3: F1, 2.21 (1.94, 2.70); F2, 2.69 (2.29, 2.97); F3, 3.42 (3.07, 3.65); and F4, 4.66 (4.40, 4.93). The elastic ratios of each METAVIR fibrosis stage at liver biopsy differed significantly from each other (F2 vs F3, $r^2 = 0.36$, $P = .02$; F3 vs F4, $r^2 = 0.41$, $P < .001$). We found a significant correlation between fibrosis stage and the elastic ratio ($\rho = 0.82$, $P < .001$). However, there was no correlation between the METAVIR activity grade and the elastic ratio ($P = .36$). The elastic ratios identified by the two examiners were strongly correlated (Fig 4) and did not differ significantly. The optimal elastic ratio cutoff values obtained for the entire population, as well as the corresponding sensitivities and specificities, are shown in Table 3. The apparent cutoff values for F ≥ 2 (2.79) and F ≥ 3 (3.25) were close, but F ≥ 3 had higher sensitivity and specificity (85.4% and 96.4%) than F ≥ 2 (82.8% and 90.9%); however, the differences were not significant (sensitivity, $P = .67$; specificity, $P = .10$). A clear cutoff value (3.93) was obtained for F = 4, with sensitivity and specificity of 90.9% and 91.5%, respectively.

Mean real-time tissue elastography liver parenchyma values were as follows: site I, 0.07 ± 0.05 (standard deviation); site II, 0.08 ± 0.045; site III, 0.08 ± 0.06; site IV, 0.09 ± 0.05; and total, 0.08 ± 0.05 ($P = .09$). The mean absolute value of the hepatic vein vessels on real-time tissue elastography did not differ significantly according to site (site I, 0.25 ± 0.14; site II, 0.25 ± 0.12; site III, 0.26 ± 0.19; site IV, 0.25 ± 0.12; and total, 0.25 ± 0.13, $P = .94$).

Relationship between Liver Elastic Ratio and Fibrosis Blood Tests

The AUCs for diagnosis of fibrosis with elastic ratio, hyaluronic acid, type IV collagen (Fig 5a), aspartate aminotransferase–to–platelet ratio index, FibroIndex, Forns score, and Hepascore (Fig 5b) were 0.95, 0.32, 0.73, 0.76, 0.76, 0.87, and 0.70, respectively (Table 4). In the multivariate stepwise regression analysis, METAVIR fibrosis stage ($P < .0001$) and prothrombin time ($P = .0013$) were

Table 3

Elastic Ratio for Determination of METAVIR F Stage

Parameter	F ≥ 2 (F1 vs F2–F4)	F ≥ 3 (F1–F2 vs F3–F4)	F = 4 (F1–F3 vs F4)
AUC	0.89	0.94	0.95
Optimal cutoff	2.73	3.25	3.93
Sensitivity (%)	82.8	85.4	90.9
Specificity (%)	90.9	96.4	91.5
Positive predictive value (%)	98.0	97.2	83.3
Negative predictive value (%)	50.0	81.8	95.6

Table 4

Results of Comparison between Real-time Elastography and Fibrosis Blood Tests

Parameter	Real-Time Elastography	APRI*	Forns Score	FibroIndex	Hepascore
AUC	0.95	0.76	0.87	0.76	0.70
Sensitivity (%)	90.9	81.8	68.2	63.6	63.4
Specificity (%)	91.5	74.4	95.8	87.5	70.8

* APRI = aspartate aminotransferase–to–platelet ratio index.

Figure 5

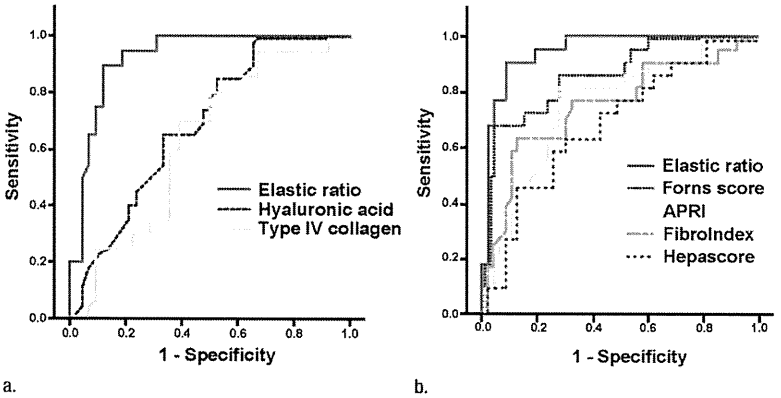

a. b.

Figure 5: **(a, b)** ROC curves for diagnosis of liver fibrosis (F4) with real-time elastography. The AUC for the diagnosis of clinically important liver fibrosis or cirrhosis (F4) by using the EUB-7500 (Hitachi Medical Systems) device is superior to the results with **(a)** blood parameters or **(b)** calculated fibrosis indexes. *APRI* = aspartate aminotransferase–to–platelet ratio index.

independently associated with the elastic ratio.

Skin Fold Thickness and BMI

Interobserver agreement for elastic ratio was excellent when the skin fold thickness was less than 20 mm and BMI was less than 25 kg/m^2. However, for patients with a skin fold thickness greater than 20 mm or a BMI greater than 25 kg/m^2, the interobserver agreement was not as good (Table 5).

Discussion

There are many reports and approaches to evaluating liver stiffness without liver biopsy. Among them, the FibroScan appears useful (23,24), but there are few reports about its reproducibility. Boursier et al (10) reported that the reproducibility of the liver hardness measurement obtained by using the FibroScan differs according to measurement position. Since the absolute value of liver stiffness at real-time tissue elastography was variable, we established a procedure to obtain reproducibility by using the signal of the small hepatic veins as a reference. Using the elastic ratio, we found no difference in reproducibility for four measurement positions. Moreover, real-time tissue elastography has other advantages compared with the FibroScan or the acoustic radiation force impulse (Appendix E1 [online]).

We checked the reproducibility of the elastic ratio derived from real-time tissue elastography. The real-time tissue elastography procedure reported previously (13) involves applying pressure in the intercostal space with a probe; thus, when the pressure applied with the probe differs, the real-time tissue elastography value changes. This means that the value of liver stiffness differs not only with each observer, but also within the same observer. Therefore, we put a probe in the intercostal space and conducted the examination with no added pressure, because when observers add pressure during measurement, observer bias may occur. The liver itself receives pressure from the heartbeat automatically, so the elastic ratio could be measured without adding any pressure with the probe. Thus, observer variability can be lessened with this procedure.

Fatty change of the liver affects the evaluation of liver stiffness with the FibroScan (11). We performed a multivariate stepwise regression analysis to identify factors that affect real-time tissue elastography. Skin fold thickness, BMI, and liver steatosis were not identified as factors affecting the elastic ratio determined by using real-time tissue elastography, while fibrosis stage was a factor. Therefore, real-time tissue elastography may measure the degree of fibrosis. Only for patients with a skin fold thickness greater than 20 mm or BMI greater than 25 kg/m^2 did the interobserver agreement have a wider range, though the difference was not significant (perhaps owing to the small

Table 5

Results according to BMI and Skin Fold Thickness

Parameter	Group 1	Group 2	Group 3	Group 4	Group 5
BMI (kg/m^2)	<19 (n = 5)	≥19 To <22 (n = 21)	≥22 To <25 (n = 27)	≥25 To <28 (n = 9)	≥28 (n = 8)
ICC	0.91	0.94	0.90	0.88	0.88
95% CI	−0.39, 1.0	0.81, 0.98	0.77, 0.96	0.36, 0.94	0.39, 0.98
Skin fold thickness (mm)	<15 (n = 15)	≥15 To <20 (n = 37)	≥20 To <25 (n = 13)	≥25 (n = 5)	...
ICC	0.95	0.92	0.83	0.81	...
95% CI	0.83, 0.98	0.84, 0.96	0.51, 0.95	−0.68, 1.00	...

sample size). The elastic ratio could be calculated for the two patients with BMIs greater than 30 kg/m^2. Further studies involving more severely obese individuals will be needed to confirm the usefulness of real-time tissue elastography for such patients.

The elastic ratio obtained by using real-time tissue elastography performed better than serum fibrosis markers and scores of fibrotic change based on blood laboratory tests. However, our study still had limitations. It is difficult to evaluate certain types of patients with B mode US, including those with thick, fat tissue under the skin; a history of abdominal operations; difficulty stopping breathing; too much liver atrophy; or a large amount of ascites. We had only two observers, each with experience with the modality, and used only one US machine. Therefore, our results might not be applicable to other individuals with less experience. Our cutoffs for determination of accuracy were based on our own results and therefore are likely overestimates of performance.

In summary, in patients with chronic hepatitis C, real-time tissue elastography allows for noninvasive assessment of fibrosis that does not vary with the sites we tested or by observer and performs better than fibrosis indexes calculated by using blood laboratory tests.

Acknowledgments: The authors thank Ravi Managuli, PhD, RDMS (Department of Bioengineering, University of Washington, Seattle, Wash), for assistance in editing the technical comments and Yoshiko Soga, MD, PhD (Pathology Division, Ehime University Hospital, Ehime, Japan), for evaluating the histologic features of liver specimens.

References

1. Lauer GM, Walker BD. Hepatitis C virus infection. N Engl J Med 2001;345(1):41–52.
2. Strader DB, Wright T, Thomas DL, Seeff LB; American Association for the Study of Liver Diseases. Diagnosis, management, and treatment of hepatitis C. Hepatology 2004; 39(4):1147–1171. [Published correction appears in Hepatology 2004;40(1):269.]
3. Cadranel JF, Rufat P, Degos F. Practices of liver biopsy in France: results of a prospective nationwide survey. For the Group of Epidemiology of the French Association for the Study of the Liver (AFEF). Hepatology 2000;32(3):477–481.
4. Pagliaro L, Rinaldi F, Craxì A, et al. Percutaneous blind biopsy versus laparoscopy with guided biopsy in diagnosis of cirrhosis: a prospective, randomized trial. Dig Dis Sci 1983;28(1):39–43.
5. Regev A, Berho M, Jeffers LJ, et al. Sampling error and intraobserver variation in liver biopsy in patients with chronic HCV infection. Am J Gastroenterol 2002;97(10):2614–2618.
6. Rousselet MC, Michalak S, Dupré F, et al. Sources of variability in histological scoring of chronic viral hepatitis. Hepatology 2005;41(2):257–264.
7. Sandrin L, Fourquet B, Hasquenoph JM, et al. Transient elastography: a new noninvasive method for assessment of hepatic fibrosis. Ultrasound Med Biol 2003;29(12): 1705–1713.
8. Friedrich-Rust M, Ong MF, Martens S, et al. Performance of transient elastography for the staging of liver fibrosis: a meta-analysis. Gastroenterology 2008;134(4):960–974.
9. Friedrich-Rust M, Wunder K, Kriener S, et al. Liver fibrosis in viral hepatitis: noninvasive assessment with acoustic radiation force impulse imaging versus transient elastography. Radiology 2009;252(2):595–604.
10. Boursier J, Konaté A, Gorea G, et al. Reproducibility of liver stiffness measurement by ultrasonographic elastometry. Clin Gastroenterol Hepatol 2008;6(11):1263–1269.
11. Fraquelli M, Rigamonti C, Casazza G, et al. Reproducibility of transient elastography in the evaluation of liver fibrosis in patients with chronic liver disease. Gut 2007;56(7): 968–973.
12. Yamakawa M, Nitta N, Shiina T, et al. High-speed freehand tissue elasticity imaging for breast diagnosis. Jpn J Appl Phys 2003;42: 3265–3270.
13. Friedrich-Rust M, Ong MF, Herrmann E, et al. Real-time elastography for noninvasive assessment of liver fibrosis in chronic viral hepatitis. AJR Am J Roentgenol 2007; 188(3):758–764.
14. Shiina T. Real time tissue elasticity imaging using the combined autocorrelation method. J Med Ultrason 1999;26(2):57–66.
15. Intraobserver and interobserver variations in liver biopsy interpretation in patients with chronic hepatitis C. The French METAVIR Cooperative Study Group. Hepatology 1994; 20(1 pt 1):15–20.
16. Bedossa P, Poynard T. An algorithm for the grading of activity in chronic hepatitis C. The METAVIR Cooperative Study Group. Hepatology 1996;24(2):289–293.
17. Wai CT, Greenson JK, Fontana RJ, et al. A simple noninvasive index can predict both significant fibrosis and cirrhosis in patients with chronic hepatitis C. Hepatology 2003;38(2):518–526.
18. Koda M, Matunaga Y, Kawakami M, Kishimoto Y, Suou T, Murawaki Y. FibroIndex, a practical index for predicting significant fibrosis in patients with chronic hepatitis C. Hepatology 2007;45(2):297–306.
19. Forns X, Ampurdanès S, Llovet JM, et al. Identification of chronic hepatitis C patients without hepatic fibrosis by a simple predictive model. Hepatology 2002;36(4 pt 1): 986–992.
20. Adams LA, Bulsara M, Rossi E, et al. Hepascore: an accurate validated predictor of liver fibrosis in chronic hepatitis C infection. Clin Chem 2005;51(10):1867–1873.
21. Fleiss JL. Statistical methods for rates and proportions. 2nd ed. New York, NY: Wiley, 1981;218.
22. Landis JR, Koch GG. The measurement of observer agreement for categorical data. Biometrics 1977;33(1):159–174.
23. Harada N, Soejima Y, Taketomi A, et al. Assessment of graft fibrosis by transient elastography in patients with recurrent hepatitis C after living donor liver transplantation. Transplantation 2008;85(1):69–74.
24. Fraquelli M, Rigamonti C. Diagnosis of cirrhosis by transient elastography: what is hidden behind misleading results. Hepatology 2007;46(1):282; author reply 282–283.

JOURNAL OF VIRAL HEPATITIS
JVH

Journal of Viral Hepatitis, 2011, **18**, 408–414 doi:10.1111/j.1365-2893.2010.01320.x

Safety and immunogenicity of hepatitis B surface antigen-pulsed dendritic cells in patients with chronic hepatitis B

S. M. F. Akbar,[1,2] S. Furukawa,[1] N. Horiike,[1] M. Abe,[1] Y. Hiasa[1] and M. Onji[1] [1]*Department of Medical Sciences, Toshiba General Hospital, Tokyo, Japan; and* [2]*Department of Gastroenterology and Metabology, Ehime University Graduate School of Medicine, Ehime Japan*

Received January 2010; accepted for publication March 2010

SUMMARY. The immune modulator capacity of antigen-pulsed dendritic cells (DC) has been documented in patients with cancers and in animal models of chronic viral infections. Cancer antigen-pulsed DC are now used for treating patients with cancer. But viral antigen-pulsed DC are not used in chronic viral-infected patients because safety of antigen-pulsed DC has not been evaluated in these patients. DC were isolated from human peripheral blood mononuclear cells by culturing with human-grade granulocyte-macrophage colony stimulating factor and interleukin-4. Human blood DC were cultured with hepatitis B surface antigen (HBsAg) for 8 h to prepare HBsAg-pulsed DC. After immunogenicity assessment of HBsAg-pulsed DC *in vitro*, five million HBsAg-pulsed DC were administered intradermally to five patients with chronic hepatitis B (CHB) 1–3 times. HBsAg-pulsed DC were immunogenic in nature because they produced significantly higher levels of interleukin-12 and interferon-γ compared to unpulsed DC ($P < 0.05$). Also, HBsAg-pulsed DC induced proliferation of HBsAg-specific T lymphocytes *in vitro*. CHB patients injected with HBsAg-pulsed DC did not exhibit generalized inflammation, exacerbation of liver damage, abnormal kidney function, or features of autoimmunity. Administration of HBsAg-pulsed DC induced anti-HBs in two patients and HBsAg-specific cellular immunity in 1 patient. This is the first study about preparation of antigen-pulsed DC using human consumable materials for treating patients with CHB. Because HBsAg-pulsed DC were safe for all patients with CHB and had immune modulation capacity in some patients, phase I and phase II clinical trials with antigen-pulsed DC in CHB and other chronic infections are warranted.

Keywords: antigen-pulsed dendritic cells, chronic hepatitis B, dendritic cells, hepatitis B surface antigen, therapeutic vaccine.

INTRODUCTION

There is no curative therapy for patients with chronic hepatitis B (CHB). Antiviral drugs are recommended to patients with CHB to attain sustained control of replication of the hepatitis B virus (HBV) and minimize liver damage [1]. However, the therapeutic efficacy of antiviral agents in patients with CHB is not complete, as most studies have reported only intermediate outcomes. A well-designed study for a National Institutes of Health consensus development conference analysed all randomized clinical trials with antiviral drugs in patients with CHB from 1989 to 2008 [2]. Results showed that no single drug treatment improved clinical outcomes or all intermediate outcomes of CHB [2], although improvements of some intermediate outcomes have been seen. However, adverse events during antiviral treatment occurred in about 50% patients. These facts support the need for a new and innovative therapeutic strategy against CHB.

Chronic HBV infection represents a viral-mediated immunological disease. Although HBV is a noncytopathic virus, patients with CHB exhibit features of liver damage and associated complications. HBV-specific immune responses are narrowly focused and weak in most patients with CHB [3]. Recent studies have also shown that impaired HBV-specific immunity and exacerbated polyclonal immune responses are related to viral persistence and liver damage in patients with CHB [4]. On the other hand, effective control

Abbreviations: ALT, alanine aminotransferase; CHB, chronic hepatitis B; CHB, chronic hepatitis B; DC, dendritic cells; HBsAg, hepatitis B surface antigen; HBV, hepatitis B virus; PBMC, Peripheral blood mononuclear cells; PBS, phosphate-buffered saline.

Correspondence: Morikazu Onji, MD, PhD., Professor and Chairman, Department of Gastroenterology and Metabology, Ehime University Graduate School of Medicine, Toon city, Ehime 791-0295, Japan.
E-mail: onjimori@m.ehime-u.ac.jp
S. M. F. Akbar and S. Furukawa contributed equally to this study.

of HBV replication and liver damage are associated with strong HBV-specific immunity in these patients [5].

Taken together, restoration of HBV-specific immunity in patients with CHB may have some therapeutic potential. In fact, a new field of clinical application of vaccines containing hepatitis B surface antigen (HBsAg) has been initiated to restore HBsAg-specific immune responses in patients with CHB [6,7]. Although safer and cheaper than commercially available antiviral drugs, restoration of HBsAg-specific immunity was not attained in patients with CHB by vaccine therapy [8].

To develop a more potent regimen of antigen-specific immune therapy, the role of antigen-presenting dendritic cells (DC) in adaptive immunity has been examined. DC are responsible for processing and presenting antigens for induction of antigen-specific immune responses in normal conditions as well as in the immune tolerance state [9,10]. Studies have shown that the phenotypes and functions of DC are distorted in patients with CHB [11,12]. Accordingly, during vaccine therapy, HBsAg may not be properly processed by DC in patients with CHB to induce HBsAg-specific immune responses.

One way to circumvent this problem is to produce antigen-pulsed DC and use them as a vaccine [9,10]. In fact, cancer antigen-pulsed DC are widely used to induce cancer-specific immunity in patients with cancer [13]. However, antigen-pulsed DC have not been produced for human use in other patient groups, and almost nothing is known about their therapeutic use outside cancer.

In our study, human blood DC were cultured with human consumable HBsAg to prepare human-grade HBsAg-pulsed DC. The functions of HBsAg-pulsed DC were assessed *in vitro*. Finally, a pilot study was carried out in patients with CHB to evaluate the safety of HBsAg-pulsed DC. The induction of HBsAg-specific immunity by HBsAg-pulsed DC was also assessed in these patients.

MATERIALS AND METHODS

Clinical trial design and study population

The study was an open-label, phase-1 safety trial in patients with CHB. Five patients with CHB were enrolled in this study. Informed written consent has been obtained from each patient. The study has been performed according to the World Medical Association declaration of Helsinki, and the procedures have been approved by the Ethical Committee of Ehime University Graduate School of Medicine, Japan. Enrolled patients did not have serological markers of hepatitis A virus, hepatitis C virus, hepatitis E virus, or human immune deficiency virus at that time of trial start. The diagnosis of CHB was made from data on clinical and serological parameters. All subjects were positive for HBsAg, HBV DNA, and antibody to hepatitis core antibody in the sera. Two subjects (patients 1 and 2) were positive for hepatitis B e antigen, whereas three subjects (patients 3, 4, and 5) were positive for antibody to hepatitis B e antigen. Anti-HBs antibodies were not detected in any patient. In four patients, liver biopsy specimens were available to make a histological diagnosis (patients 1, 2, 3, and 5). All of them had moderate levels of hepatitis. Levels of fibrosis were mild in patients 1 and 2 and severe in patients 3 and 5. These patients were attending our university hospital for regular follow-up and treatment. The clinical profiles of patients before administration of HBsAg-pulsed DC are shown in Table 1. Levels of alanine aminotransferase (ALT) in the sera were elevated in three patients (patients 1, 2, and 5) and within normal limits in patients 3 and 4. No patient showed any feature of general inflammation (assessed from serum levels of C-reactive protein) or abnormal kidney function.

Isolation of DC from peripheral blood and loading of HBsAg in vitro

Isolation of human blood DC and production of HBsAg-pulsed DC were carried out as reported previously [14]. A special room was assigned for cell cultures, and DC were isolated from one person at a time. All reagents used for cell culture studies were free from endotoxin and toxoplasma. Peripheral blood mononuclear cells (PBMC) were isolated from freshly drawn heparinized whole blood, washed three times, and resuspended in RPMI 1640 (Nipro, Osaka, Japan) plus 10% autologous serum. DC were enriched from an adherent population of PBMC, as described previously [14]. PBMC were cultured in RPMI 1640 plus 10% autologous sera and human-grade granulocyte-macrophage stimulating factor (800 U/mL) and interleukin (IL)-4 (400 U/ml) (Pepro Tech EC Ltd., London, UK) for 7 days. DC were retrieved from the culture and washed three times with phosphate-buffered saline (PBS). The expressions of DC-related markers on human DC were checked by direct flow cytometry.

To produce HBsAg-pulsed DC, blood DC were cultured with a commercially available HB vaccine containing 10 μg of HBsAg (Heptavax-II, subtype adw, Banyu Pharmaceutical Co., Tokyo, Japan) for 8 hours. After the end of culture, DC were pelleted and washed five times in PBS. After the last wash, the final solutions were collected and preserved at −20 °C to assess if there was any free HBsAg in HBsAg-pulsed DC. As a control, human blood DC were cultured in RPMI 1640 plus autologous sera for 8 h.

Analyses of phenotype and functions of DC

The expression of HLA DR and CD86 on unpulsed DC and HBsAg-pulsed DC were assessed by direct flow cytometry using fluorescein isothiocyanate-conjugated monoclonal antibody to human HLA DR (Clone L243) and phycoerythrin-conjugated monoclonal antibody to human CD86 (clone 2331 [FUN-1]) (all from BD Pharmingen, San Jose,

Table 1 Clinical profiles of patients with chronic hepatitis B before administration of HBsAg-pulsed DC

	Patient no.				
	1	2	3	4	5
Age (years)	36	30	35	48	57
Sex	Male	Male	Male	Female	Male
Alanine aminotransferase (5–48 IU/L)*	169	83	35	31	95
Asparate aminotransferase (6–45 IU/L)	76	52	30	40	80
Prothrombin time (80–120%)	112.6	100	84	85.3	108.6
Creatinine (0.61–1.04 mg/dL)	0.6	0.7	0.6	0.6	0.9
Blood urea nitrogen (6–20 mg/dL)	8.0	12.0	11.0	11.0	14.0
C-reactive protein (<0.30 mg/dL)	0.04	0.05	0.03	0.03	0.04
Antinuclear antibody (<40)	–	–	–	–	–
Histology					
Activity	A2	A1	A2	ND	A2
Fibrosis	F1	F1	F3	ND	F3
HBV DNA (Log genomic equivalent)	7.2	7.5	<3.7	4.8	7.5
Hepatitis B surface antigen (IU/ml)	+	+	+	+	+
Hepatitis B e antigen (S/CO)	+	+	–	–	–
Antibody to hepatitis B e antigen	–	–	+	+	+
Antibody to hepatitis B core antigen	+	+	+	+	+
Antibody to hepatitis B surface antigen	–	–	–	–	–

HBV, hepatitis B virus.
*Levels in parenthesis indicate normal range.

CA, USA). Data acquisition and analysis were performed on fluorescein-activated cell sorter (Becton Dickinson Biosciences, San Jose, CA, USA) [14].

T-cell stimulatory capacity and HBsAg-specific proliferative capacity of DC were assessed in allogenic mixed leucocyte reaction and antigen-specific lymphoproliferative assays. Human blood DC were cultured with allogenic T cells, or autologous T cells were cultured with unpulsed or HBsAg-pulsed DC for 104 h, and then [^{3}H]-thymidine was added to the cultures. The cultures were done for an additional 16 h. The cultures were then harvested using a semiautomatic harvester, and the level of incorporation of [^{3}H]-thymidine was shown as counts per minute in a scintillation counter (Beckman LS 6500, Beckman Instruments, Inc., Fullerton, CA, USA) [14]. Data were also expressed as counts per minute or a stimulation index that was calculated by dividing the counts per minute in culture containing HBsAg-pulsed DC with that of unpulsed DC. A stimulation index >2.0 was considered a significant proliferation.

Levels of IL-12 and interferon (IFN)-γ in samples were measured by an enzyme-linked immunosorbent assay (ELISA) using commercial kit (BD Pharmingen).

Estimation of HBsAg and anti-HBs

To estimate levels of HBsAg and anti-HBs, samples were sent to commercial companies (Special Reference Laboratory, Osaka, Japan). The estimation was performed using the chemiluminescence enzyme immunoassay method. Detection limits of HBsAg and anti-HBs were 0.2 ng/mL and 3.0 mIU/mL, respectively. Some samples were sent to a second commercial company (Shikoku Chuken Co, Matsuyama, Japan) for further confirmation.

Immunization of CHB patients with HBsAg-pulsed DC

HBsAg-pulsed DC were suspended in PBS and placed in two syringes. In one syringe, 20 μL of PBS containing 2×10^5 HBsAg-pulsed DC was suspended. In a second syringe, 5 million HBsAg-pulsed DC were diluted in 250 μL of PBS. First, 2×10^5 HBsAg-pulsed DC in 20 μL of PBS were injected at the anterior part of forelimb of patients with CHB to see if there was any hypersensitivity reaction. After 15 minutes, patients were injected intradermally in the deltoid region with 5 million HBsAg-pulsed DC. The patients with CHB were allowed to rest for 30 min. They were then monitored periodically for temperature, pulse rate, blood pressure, and respiratory rate for the first 24 h. Blood was collected from all patients before immunization and at different times after immunization with HBsAg-pulsed DC. Parameters of generalized inflammation, liver function test, kidney function test, and autoantibodies were checked in all patients at different times after the administration of HBsAg-pulsed DC. Patients received 1, 2, or 3 injections over 4 months. The immunization schedule for each patient is shown in Fig. 1.

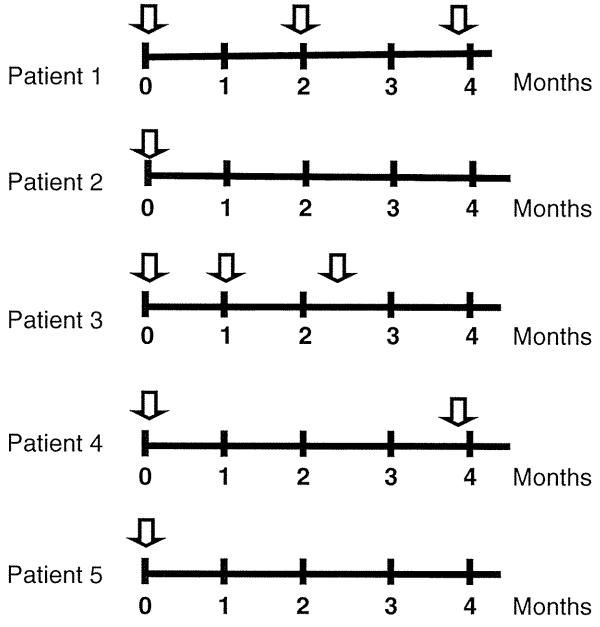

Fig. 1 Immunization schedule with HBsAg-pulsed DC in patients with chronic hepatitis B (CHB). HBsAg-pulsed DC were administered 1–3 times (arrows).

Statistical analysis

Values are represented as mean ± standard deviation (SD). Data were analysed by unpaired t tests if data were normally distributed and by Mann–Whitney rank-sum test if they were skewed. Differences were considered significant if $P < 0.05$.

RESULTS

Features of human blood DC

As a preliminary study, we first isolated DC from patients with CHB and pulsed with HBsAg, as described previously [15]. Flow cytometry analysis revealed that the frequencies of contaminating T lymphocytes (CD3-positive cells), B lymphocytes (CD19, 20, 21-positive cells), monocytes (CD14-positive cells), and natural killer cells (CD56-positive cells) were less than 5% of the total DC (data not shown). DC from patients with CHB expressed DC-related antigens, such as HLA-A, B, C, HLA DR, CD86, and CD40. A functional study showed that DC from patients with CHB stimulated allogenic T cells in a dose-dependent manner (Fig. 2).

Characterization of HBsAg-pulsed DC from patients with CHB

During preliminary experiments, we checked two features of HBsAg-pulsed DC for this clinical trial: (i) there should be no free HBsAg in HBsAg-pulsed DC and (ii) HBsAg-pulsed DC should be immunogenic in nature so that it can induce

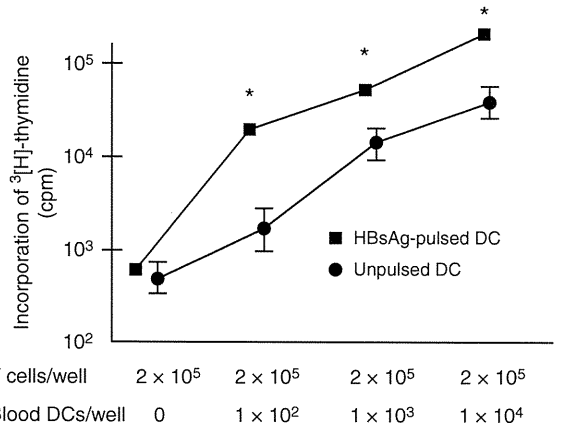

Fig. 2 DC from patients with chronic hepatitis B (CHB) stimulated allogenic T cells in a dose-dependent manner. However, HBsAg-pulsed DC had significantly higher capacities to induce blastogenesis of T cells compared with unpulsed DC. Data from 5 separate experiments are shown. cpm, counts per minute. *$P < 0.05$.

HBsAg-specific immune responses *in vivo*. No HBsAg was detected in the final wash solution of HBsAg-pulsed DC. Levels of IL-12 were significantly increased in culture containing HBsAg-pulsed DC from patients with CHB (156.2 ± 20.7 pg/mL) compared to unpulsed DC (29.2 ± 9.8 pg/mL) from patients with CHB ($P < 0.05$). Similarly, levels of IFN-γ were significantly increased in culture containing HBsAg-pulsed DC (232.4 ± 24.1 pg/mL) from patients with CHB compared to unpulsed DC (80.5 ± 12.9 pg/mL) from patients with CHB ($P < 0.05$). HBsAg-pulsed DC also induced significantly higher levels of blastogenesis of T cells compared to unpulsed DC (Fig. 2). Also, HBsAg-pulsed DC induced significant proliferation of HBsAg-specific T lymphocytes *in vitro* (data not shown). After confirming these points, we prepared HBsAg-pulsed DC for administration to patients with CHB.

Safety of HBsAg-pulsed DC in patients with CHB

No immediate or delayed inflammatory or allergic reaction was detected at the injection site of HBsAg-pulsed DC in any patient. No patient complained of any allergic reaction or fever after immunization with HBsAg-pulsed DC. Different parameters of blood biochemistry, liver and kidney functions, and immunological statuses of all patients with CHB were checked periodically, and data during follow-up period after the end of administration of HBsAg-pulsed DC in these patients have been shown in Table 2. There was no significant change in levels of C-reactive protein or other parameters of general features of inflammation because of administration of HBsAg-pulsed DC. In addition, parameters of kidney function were within normal ranges in all patients after the administration of HBsAg-pulsed DC. Features of autoimmunity or autoantibodies were not detected in any patient.

Table 2 Clinical profiles of patients with chronic hepatitis B during follow-up after completion of administration of HBsAg-pulsed DC

	Patient no. 1		Patient no. 2		Patient no. 3		Patient no. 4		Patient no. 5	
	1M*	3M	1M	3M	1M	3M	1M	3M	1M	3M
Alanine aminotransferase (5–48 IU/L)	171	147	57	36	37	30	43	41	109	72
Asparate aminotransferase (6–45 IU/L)	89	73	37	28	32	38	33	35	88	58
Prothrombin time (80–120%)	113.8	99.5	80.3	98.9	97	95	81.5	84.5	103.4	12.1
Creatinine (0.61–1.04 mg/dL)	0.7	0.7	0.7	0.7	0.6	0.6	0.6	0.6	0.9	1.0
Blood urea nitro- gen (6–20 mg/dL)	10	7	8	9	10	8	9	9	13	10
C-reactive protein (<0.30 mg/dL)	0.03	0.03	0.03	0.03	0.02	0.03	0.03	0.04	0.04	0.03
Antinuclear antibody (<40)	–	–	–	–	–	–	–	–	–	–
HBV DNA (Log genomic equivalent)	7.1	7.0	6.3	5.5	<3.7	<3.7	3.8	4.0	6.8	6.5

HBV, hepatitis B virus.
*Indicates month after end of last administration with hepatitis B surface antigen (HBsAg)-pulsed dendritic cells (DC). 1M; 1 month after completion of administration of HBsAg-pulsed DC, 3M; 3 months after completion of administration of HBsAg-pulsed DC.

Effect of HBsAg-pulsed DC on serum ALT levels

ALT levels just before the administration of HBsAg-pulsed DC are shown in Table 1. Because of the CHB, patients exhibited fluctuating ALT levels. The highest ALT level was <300 IU/L in all patients. There was no significant alteration in serum ALT levels because of administration of HBsAg-pulsed DC (Table 2).

Impact of HBsAg-pulsed DC as a therapeutic vaccine

The main aim of this study was to evaluate whether immunogenic HBsAg-pulsed DC can be prepared from DC of patients with CHB. The next goal was to assess whether administration of HBsAg-pulsed DC was safe. Although this study was not designed to assess the therapeutic potential of HBsAg-pulsed DC in patients with CHB, we checked levels of HBsAg, HBeAg negativity, and anti-HBe seroconversion in all patients. Administration of HBsAg-pulsed DC did not cause any major change in these parameters (data not shown). As shown in Table 2, the levels of HBV DNA were decreased slightly, but not significantly, because of administration of HBsAg-pulsed DC in these patients. Adverse effects were not detected in any patient. For example, three patients were anti-HBe positive, and the administration of HBsAg-pulsed DC did not cause reappearance of HBeAg in any patient.

Increased cytokine production by immunocytes of patients with CHB because of administration of HBsAg-pulsed DC

DC and T cells of patients with CHB were collected before and after the administration of HBsAg-pulsed DC and cultured in autologous mixed leucocyte reaction. Levels of IL-12 (before, 32.3 ± 5.2 pg/mL; after, 145 ± 9.2 pg/mL) and INF-γ (before, 21.7 ± 3.2 pg/mL; after, 154 ± 11.8 pg/mL) were significantly higher in culture supernatants after the administration of HBsAg-pulsed DC compared to before administration ($P < 0.05$).

HBsAg-specific immunity because of administration of HBsAg-pulsed DC

Administration of HBsAg-pulsed DC induced anti-HBs in two patients (patients 1 and 3). Anti-HBs were detected 1 month after HBsAg-pulsed DC administration in patient 1 and 2 months after HBsAg-pulsed DC administration in patient 3. Levels of anti-HBs increased progressively for 5 months in patient 1 and then started to decline. In contrast, levels of anti-HBs remained similar over time in patient 3 (Fig. 3).

HBsAg-specific cellular immunity in patient 1

HBsAg-specific T cells proliferation was not detected in any patient before study commencement. However, HBsAg-specific cellular immune responses 2 months after the third injection of HBsAg-pulsed DC were detected in patient 1 (Fig. 4).

DISCUSSION

Potent antiviral and antitumour effects of antigen-pulsed DC have been documented in animal models of human diseases since the 1980s. The first clinical trial of cancer antigen-pulsed DC was conducted in patients with cancer in 1996 [15]. Several clinical trials with cancer antigen-pulsed DC are ongoing worldwide [13]. It is expected that viral antigen-pulsed DC may be an effective immune therapy in patients with chronic viral infections, but such approaches have not yet been attempted clinically.

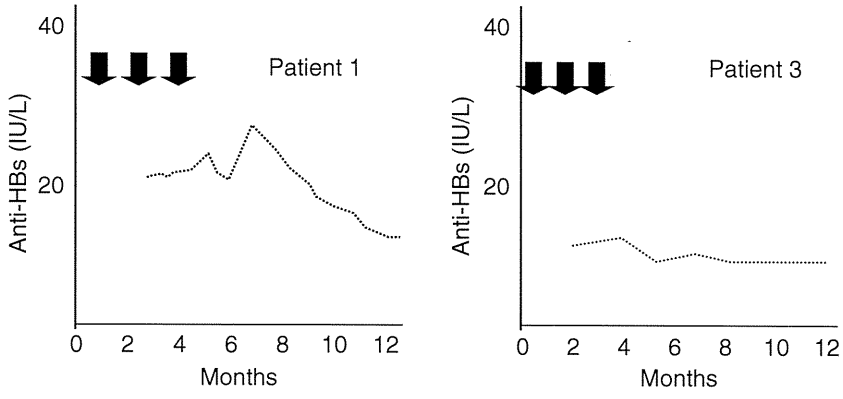

Fig. 3 Anti-HBs in 2 patients with chronic hepatitis B (CHB) after administration (arrows) of HBsAg-pulsed DC.

To treat patients with cancer, DC have been loaded with tumour-associated antigens, crude tumour products, tumour RNA, and other tumour-derived products *in vitro* [13,16]. The resultant cancer antigen-pulsed DC have been injected into patients with cancer, especially in those with advanced cancer. Many of these patients were immune compromised because they were in terminal stage of cancer. However, almost all patients with chronic viral infections are immune competent. Thus, a systemic and cautious approach is needed to prepare viral antigen-pulsed DC and initiate a clinical trial.

In this study, we used HBsAg, a well-known protein of HBV, to load human blood DC. As the safest source of HBsAg, we used a prophylactic hepatitis B vaccine. We showed that there was no free HBsAg in HBsAg-pulsed DC. This is important because if free antigen is present in HBsAg-pulsed DC, it will be difficult to assess the real effects of antigen-pulsed DC *in vivo* because free HBsAg may also induce immune responses *in vivo*. We also found that HBsAg-pulsed DC produced significantly higher levels of IL-12 and IFN-γ, two immune stimulatory cytokines compared to unpulsed DC. Furthermore, we checked for any contamination in HBsAg-pulsed DC. When we reproducibly produced immunogenic HBsAg-pulsed DC without any contamination, we moved forward to conduct this pilot study.

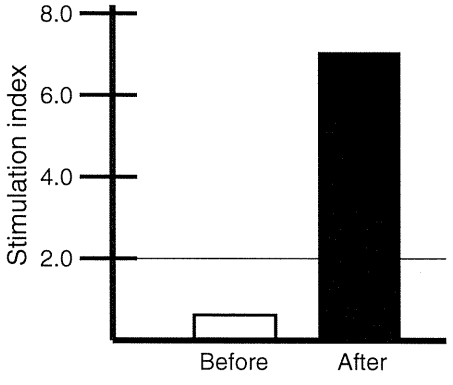

Fig. 4 HBsAg-specific cellular immune responses were seen after the third immunization of HBsAg-pulsed DC in patient 1.

Antigen-specific humoral and cellular immune responses were detected in 2 and 1 patients, respectively, because of administration of HBsAg-pulsed DC. It is premature to comment about the therapeutic efficacy of HBsAg-pulsed DC in this study because this is a pilot study. Indeed, there are several opportunities to improve our protocol. As the safest form of HBsAg, we used HBsAg in an HB vaccine. This allowed us to use a maximum of 10 μg of HBsAg to maximize DC viability during preparation of HBsAg-pulsed DC. In the future, human consumable recombinant HBsAg in larger doses may be used for preparing antigen-pulsed DC. We used only 5 million HBsAg-pulsed DC, as this was the first clinical trial of this nature. In the future, a dose escalation study with HBsAg-pulsed DC should be conducted. In addition, the number of patients needs to be increased.

Our study represents an initial effort to develop antigen-specific immune therapy for patients with CHB. We have systematically prepared HBsAg-pulsed DC and used them in normal volunteers [17] and hepatitis B vaccine nonresponders [14]. HBsAg-pulsed DC were completely safe and immunogenic in normal volunteers and hepatitis B vaccine nonresponders, who have been followed for 5 years after the administration of HBsAg-pulsed DC [14,17]. Finally, we used HBsAg-pulsed DC in patients with CHB and also confirmed the safety of this treatment. However, this is a small study, and there are several limitations that affect the interpretation of the findings. First, we only included five patients. In addition, patients were immunized 1–3 times with HBsAg-pulsed DC. However, this was a pilot study to demonstrate the use of DC-based therapy in immune competent persons with a chronic viral infection. We are now planning to prepare other HBV-related antigen-pulsed DC for patients with CHB because only HBsAg-pulsed DC may not be the best therapeutic option. Hepatitis B core antigen-pulsed DC may be required to restore therapeutic HBV-specific immunity. Also, antigen-pulsed DC may be used as a part of combination therapy with antiviral drugs in patients with CHB [18]. Finally, the concept and techniques used in this

study may be used to prepare antigen-pulsed DC for other chronic infections.

REFERENCES

1 Fattovich G. Natural history and prognosis of hepatitis B. *Semin Liver Dis* 2003; 23: 47–58.
2 Shamiliyan TA, MacDonald R, Shaukat A *et al.* Antiviral therapy for adults with chronic hepatitis B: a systemic review for a national institute of health consensus development conference. *Ann Intern Med* 2009; 150: 111–124.
3 Rehermann B. Immune responses to hepatitis B virus infection. *Semin Liver Dis* 2003; 23: 21–37.
4 Bertoletti A, Maini MK. Protection or damage: a dual role for the virus-specific cytotoxic T lymphocyte response in hepatitis B and C infection? *Curr Opin Microbiol* 2000; 3: 387–392.
5 Maini MK, Boni C, Lee CK *et al.* The role of virus-specific CD8(+) cells in liver damage and viral control during persistent hepatitis B virus infection. *J Exp Med* 2000; 191: 1269–1280.
6 Pol S, Driss F, Michel ML *et al.* Specific vaccine therapy in chronic hepatitis B infection. *Lancet* 1994; 344: 342.
7 Pol S, Nalpas B, Driss F *et al.* Efficacy and limitations of a specific immunotherapy in chronic hepatitis B. *J Hepatol* 2001; 34: 917–921.
8 Inchauspé G, Michel ML. Vaccines and immunotherapies against hepatitis B and hepatitis C viruses. *J Viral Hepat* 2007; 14(Suppl. 1): 97–103.
9 Steinman RM. Dendritic cells: understanding immunogenicity. *Eur J Immunol* 2007; 37(Suppl. 1): S53–S60.
10 Onji M, Akbar SM, eds. Dendritic Cells in Clinics. Tokyo: Springer, 2008.
11 Arima S, Akbar SMF, Michitaka K *et al.* Impaired function of antigen-presenting dendritic cells in patients with chronic hepatitis B: localization of HBV DNA and HBV RNA in blood DC by *in situ* hybridization. *Int J Mol Med* 2003; 11: 169–174.
12 van der Molen RG, Sprengers D, Binda RS *et al.* Functional impairment of myeloid and plasmacytoid dendritic cells of patients with chronic hepatitis B. *Hepatology* 2004; 40: 738–746.
13 Banchereau J, Paluka K. Dendritic cells as therapeutic vaccines against cancer. *Nature Rev Immunol* 2005; 3: 296–306.
14 Akbar SM, Furukawa S, Yoshida O *et al.* Induction of anti-HBs in HB vaccine nonresponders *in vivo* by hepatitis B surface antigen-pulsed blood dendritic cells. *J Hepatol* 2007; 47: 60–67.
15 Hsu FJ, Benike C, Fagnoni F *et al.* Vaccination of patients with B-cell lymphoma using autologous antigen-pulsed dendritic cells. *Nat Med* 1996; 2: 52–58.
16 Akbar SMF, Abe M, Yoshida M *et al.* Dendritic cell-based therapy as a multidisciplinary approach to cancer treatment: present limitation and future scopes. *Curr Med Chem* 2006; 13: 3113–3119.
17 Akbar SMF, Furukawa S, Onji M *et al.* Safety and efficacy of hepatitis B surface antigen-pulsed dendritic cells in human volunteers. *Hepatol Res* 2004; 29: 136–141.
18 Sprengers D, Janssen HL, Kwekkeboom J, Niesters HG, de Man RA, Schalm SW. *In vivo* immunization following virus suppression: a novel approach for inducing immune control in chronic hepatitis B. *J Viral Hepat* 2003; 10: 7–9.

Clinical & Experimental Immunology
The Journal of Translational Immunology

Clinical and Experimental Immunology ORIGINAL ARTICLE doi:10.1111/j.1365-2249.2011.04445.x

Immunosuppressive functions of hepatic myeloid-derived suppressor cells of normal mice and in a murine model of chronic hepatitis B virus

S. Chen,* S. M. F. Akbar,*† M. Abe,* Y. Hiasa* and M. Onji*
*Department of Gastroenterology and Metabology, Ehime University Graduate School of Medicine, Toon City, Ehime, and †Department of Medical Sciences, Toshiba General Hospital, Tokyo, Japan

Accepted for publication 2 June 2011
Correspondence: Morikazu Onji, Department of Gastroenterology and Metabology, Ehime University Graduate School of Medicine, Shitsukawa 454, Toon City, Ehime 791-0295, Japan.
E-mail: sheikh.akbar@po.toshiba.co.jp

Summary

The immunosuppressive state of tumour-bearing hosts is attributable, at least in part, to myeloid-derived suppressor cells (MDSC). However, the role of MDSC in physiological conditions and diseases other than cancer has not been addressed. As the liver is a tolerogenic organ, the present study attempted to localize and assess functions of hepatic MDSC in a normal liver and in a murine model of chronic hepatitis B virus (HBV) infection. MDSC was identified in the liver of normal mice and HBV transgenic mice (TM) as $CD11b^+$ $Gr1^+$ cells by dual-colour flow cytometry. Highly purified populations of MDSC and their subtypes were isolated by fluorescence-activated cell sorting. The functions of MDSC and their subtypes were evaluated in allogenic mixed lymphocyte reaction (MLR) and hepatitis B surface antigen (HBsAg)-specific T cell proliferation assays. Normal mice-derived liver MDSC, but not other myeloid cells ($CD11b^+$ $Gr1^-$), suppressed T cell proliferation in allogenic MLR in a dose-dependent manner. Alteration of T cell antigens and impaired interferon-γ production seems to be related to MDSC-induced immunosuppression. In HBV TM, the frequencies of liver MDSC were about twice those of normal mice liver (13·6 ± 3·2% *versus* 6·05 ± 1·21%, $n = 5$, $P < 0·05$). Liver-derived MDSC from HBV TM also suppressed proliferative capacities of allogenic T cells and HBsAg-specific lymphocytes. Liver MDSC may have a critical role in maintaining homeostasis during physiological conditions. As liver MDSC had immunosuppressive functions in HBV TM, they may be a target of immune therapy in chronic HBV infection.

Keywords: hepatic immunity, hepatitis B virus, homeostasis, immunosuppression, myeloid-derived suppressor cells

Introduction

Myeloid-derived suppressor cells (MDSC) are a phenotypically heterogeneous cell population that includes mature myeloid cells as well as immature myelomonocytic precursors [1]. Excessive numbers of MDSC have been detected in the blood of patients with head and neck squamous cell carcinoma [2] and mice with lung tumours [3]. These cells have been detected in bone marrow, spleen and peripheral blood, within primary and metastatic solid tumours and in lymph nodes in tumour-bearing mice [1,4–6]. Functionally, MDSC suppresses the function of T cells, block natural killer (NK) cell cytotoxicity [7], modulate macrophages to an immunosuppressive M2 phenotype [8,9] and induce the development of regulatory T cells [10] in tumour-bearing hosts.

Although considerable insight has been developed into the immunosuppressive functions of MDSC in cancers, little is known about these cells in physiological conditions. However, many parenchymal organs of the body maintain an immune tolerogenic state in physiological conditions. The liver is a typical example of a tolerogenic organ in physiological condition. Different food products, inflammatory substances, allergens and drug metabolites constantly enter the liver through the gut or bloodstream. Under physiological conditions, the liver induces immunological tolerance to these substances to prevent detrimental immune reactions [11,12]. The inherent tolerogenic property of the liver is attributable to a unique hepatic microenvironment. However, unexplored immunocytes such as MDSC may have a role in this regard.

This study was performed to detect MDSC in normal mice liver by dual-colour flow cytometry. The subtypes of liver MDSC and expressions of surface antigens on different liver MDSC subtypes were elucidated. Functional assessment was accomplished to assess whether MDSC are immunosuppressive in normal mice. Also, the extents of immunosuppressive potentials of two subtypes of liver MDSC were compared. Finally, we evaluated functions of liver MDSC from hepatitis B virus (HBV) transgenic mice (TM), an animal model of virus-induced immunosuppression [13], to determine the clinical implications of MDSC in chronic viral infections.

Materials and methods

Mice

Seven-week-old male C57BL/6JJcl and C3H/HeNJcl mice were purchased from Clea Japan, Inc. (Tokyo, Japan). HBV-TM (official designation: l.2HB-BS10) were produced by microinjecting a partial tandem duplication of the complete HBV genome into fertilized eggs of C57BL/6 mice [14]. HBV TM produced hepatitis B surface antigen (HBsAg), hepatitis B e antigen, and HBV DNA in sera. HBV-related mRNAs were expressed in the liver, kidney and testis [14]. Normal C57BL/6JJcl (7-week-old male) mice were immunized twice with intraperitoneal HBsAg (10 μg, Heptavax-II, subtype adw; Banyu Pharmaceutical, Osaka, Japan) at an interval of 4 weeks to induce HBsAg-specific lymphocytes. Normal mice and HBV TM were housed separately in polycarbonate cages in a temperature-controlled room (23 ± 1°C) with a 12-h light/dark cycle in a pathogen-free animal housing facility at Ehime University Graduate School of Medicine. All animals received humane care, and study protocols were in compliance with the institution's guidelines. An animal experimental board of Ehime University approved the study.

Isolation of spleen cells and liver non-parenchymal cells (NPCs)

To produce a single cell suspension from the spleen, spleens were cut into pieces and passed through a 40-μm pore-size nylon filter (BD Falcon, Durham, NC, USA); the resulting cells were collected and suspended in a culture medium (RPMI-1640 medium; GIBCO® Invitrogen, Carlsbad, CA, USA) plus 10% fetal bovine serum (GIBCO® Invitrogen) [15,16].

To retrieve liver NPCs, liver tissues were cut into pieces, homogenized, passed through 70-μm pore-size steel meshes (Morimoto Yakuhin Co., Matsuyama, Japan) and suspended in 35% Percoll (Sigma Chemical, St Louis, MO, USA). After centrifugation for 15 min at 450 ***g*** at room temperature, a high-density cell pellet was collected and suspended in a culture medium [15,16].

Isolation of T lymphocytes and dendritic cells (DC)

T lymphocytes and DC were isolated from mouse spleen, as described previously [15,16]. T lymphocytes were isolated from C3H/He mice spleen single-cell suspension by a negative selection column method using a mouse pan T isolation kit (Miltenyi Biotec, Bergisch Gladbach, Germany). DC were isolated from C57BL/6J mice spleen by positive selection column method using a mouse CD11c Microbeads (Miltenyi Biotec) based on the manufacturer's instructions.

Flow cytometry and cell sorting

To identify MDSC and their subtypes, allophycocyanin (APC) anti-mouse Gr-1 (clone RB6-8C5) and phycoerythrin (PE) anti-mouse CD11b (clone M1/70) were used (BD Biosciences, San Jose, CA, USA). In order to assess the expressions of surface antigens on subtypes of MDSC, fluorescein isothiocyanate (FITC) anti-mouse Ly-6G (clone 1A8), Ly-6C (clone AL-21), CD31 (clone 390) were purchased from BD Biosciences, and F4/80 (clone BM8) from eBioscience (San Diego, CA, USA). PE anti-mouse Cytotoxic T-Lymphocyte Antigen 4 (CTLA-4) (clone UC10-4F10-11), PD-1 (clone J43), CD62L (clone MEl-14) and CD40L (clone MR1) (BD Biosciences) were used to evaluate expressions of activation/exhaustion markers on T cells. For intracellular cytokine staining, cells were lysed using Fixation and Permeabilization Kit (Invitrogen, Carlsbad, CA, USA) based on the manufacturer's instructions, and stained with APC anti-mouse interferon (IFN)-γ (clone XMG 1·2) (eBioscience). The corresponding isotype antibodies were used with all the samples as controls. Flow cytometry was performed on a Becton Dickinson fluorescence activated cell sorter (FACS)Calibur using CellQuest Software (Becton Dickinson, Franklin Lakes, NJ, USA). Data analysis was performed by using FlowJo software (TreeStar Corporation, Ashland, OR, USA).

To isolate MDSC and MDSC subtypes, spleen cells and liver NPCs were stained with monoclonal antibodies to CD11b and Gr1 and were sorted with the BD FACSAria™ Cell Sorting System (Becton Dickinson). $CD11b^+$ $Gr1^-$ cells were also sorted from liver NPCs and spleen cells suspensions by similar methods. All sorted cells were of purity above 98%.

The expressions of different surface antigens on MDSC and T cells were shown as relative frequencies among total cell populations or mean fluorescence intensity (MFI).

T cell suppression assay

C3H/HeN spleen T lymphocytes were mixed with C57BL/6J spleen DC and co-cultured in the absence or presence of sorted MDSC at different ratios to evaluate the suppressive function of MDSC in allogenic mixed leucocyte reaction (MLR). Spleen cells were also stimulated with concanavalin A (ConA, 1 μg/ml; Sigma). Spleen cells from HBsAg-injected

C57BL/6J mice were cultured with or without HBsAg in the absence or presence of MDSC to assess the role of MDSC on HBsAg-specific lymphocyte proliferation. The culture conditions are described in detail elsewhere [15–17]. All cultures were performed in 96-well U-bottomed plates (Corning Inc., New York, NY, USA). [^{3}H]-thymidine (1·0 μCi/ml; Amersham Biosciences, Little Chalfont, Buckinghamshire, UK) was diluted in sterile RPMI-1640 and added to the cultures for the last 16 h and harvested automatically by a multiple cell harvester (Labo Mash; Futaba Medical, Osaka, Japan) onto a filter paper (Labo Mash 101–10; Futaba Medical). The levels of incorporation of [^{3}H]-thymidine were determined in a liquid scintillation counter (Beckman LS 6500; Beckman Instruments, Inc., Fullerton, CA, USA). The levels of T cell proliferation were enumerated as counts per minute (cpm). The level of cpm in culture containing only T cells was considered background proliferation and expressed as a stimulation index (SI) of 1·0. The levels of T cell proliferation in allogenic MLR were estimated by dividing the cpm in cultures containing T cells with DC or MDSC or other myeloid cells with the cpm of control cultures containing only T cells. The levels of proliferation of HBsAg-specific lymphocytes were estimated by dividing the cpm in cultures containing lymphocytes/HBsAg or MDSC with the cpm of control cultures containing T cells and an irreverent antigen, pyruvate dehydrogenase complex (Sigma Aldrich Corporation, St Louis, MO, USA) [17].

Statistical analysis

Data were expressed as mean ± standard deviation (s.d.). In all statistical analysis, data of two groups were analysed by Student's *t*-tests if they were normally distributed and by the Mann–Whitney rank-sum test if they were skewed. Differences were considered significant at $P < 0·05$ between two groups.

Results

Enumeration of MDSC and their subtypes

MDSC was detected in the liver and spleen of normal mice and HBV TM as cells expressing both CD11b and Gr1 (Fig. 1a). In normal mice, the proportions of liver MDSC were significantly higher than in the spleen (6·05 ± 1·21% *versus* 1·33 ± 0·50%, respectively; $P < 0·05$, $n = 5$). MDSC consisted of two main subtypes: CD11b$^+$ Gr1^{high} (shown by circle in Fig. 1a) and CD11b$^+$ GR1^{dim} (shown by square in Fig. 1a). In the spleen, the proportions of both subtypes of MDSC were almost comparable (Fig. 1b). However, the main subtype of MDSC in the liver was CD11b$^+$ Gr1^{dim} (Fig. 1c). This was seen in both normal mice and HBV TM (Fig. 1c).

The expression of different surface antigens showed considerable variations between MDSC subtypes of the liver (Fig. 2). The relative ratio of different surface antigens on two subtypes of liver MDSC was shown in Fig. 2b. Ly6G was expressed in most CD11b$^+$ Gr1^{high} MDSC, whereas CD31 and F4/80 were detected mainly in CD11b$^+$ Gr1^{dim} MDSC (Fig. 2b). The levels of expression of Ly6G (assessed by MFI) were significantly higher in CD11b$^+$ Gr1^{high} MDSC than in CD11b$^+$ Gr1^{dim} MDSC (Fig. 2c). Conversely, the levels of expression of Ly6C were significantly higher in CD11b$^+$ Gr1^{dim} MDSC compared to CD11b$^+$ Gr1^{high} MDSC (Fig. 2c).

Immunosuppressive capacities of normal mouse liver-derived MDSC, but not by non-MDSC myeloid cells

MDSC from normal liver suppressed T cell proliferation in allogenic MLR in a dose-dependent manner. In allogenic MLR, the levels of T cell proliferation were 87·0 ± 5·3 SI ($n = 5$). As shown in Fig. 3a, when 1×10^4 MDSC were added to the culture, the levels of blastogenesis decreased to 73·4 ± 7·8 SI ($n = 5$) ($P < 0·05$). The levels of blastogenesis decreased further to 60·7 ± 5·6 SI ($n = 5$) ($P < 0·05$) and 45·3 ± 2·6 SI ($n = 5$) ($P < 0·05$) when 2×10^4 and 3×10^4 MDSC were added to the cultures, respectively (Fig. 3a). However, increased proliferations of T cells were seen in allogenic MLR when non-MDSC myeloid cells (CD11b$^+$Gr1$^-$ cells) from normal mouse liver were added to the cultures (Fig. 3a).

As MDSC from mouse liver suppressed T cell proliferation, it was important to assess if there is any difference in T cell suppressive capacity between MDSC subtypes. In allogenic MLR, the levels of T cell proliferation were 86·0 ± 8·7 SI ($n = 5$) when 2×10^5 T cells from C3H/HeN mice were cultured with 1×10^4 DC from C57BL/6J mice. When 3×10^4 CD11b$^+$ Gr1^{high} MDSC were added to the culture, the levels of blastogenesis decreased to 62·1 ± 9·2 SI ($n = 5$) ($P < 0·05$, compared to cultures without MDSC). The levels of blastogenesis decreased to 40·2 ± 4·1 SI ($n = 5$) when 3×10^4 CD11b$^+$ Gr1^{dim} MDSC were added to the culture ($P < 0·05$, compared to cultures containing CD11b$^+$ Gr1^{high} MDSC). Taken together, CD11b$^+$ Gr1^{dim} MDSC exhibited significantly higher T cell suppressive capacities than CD11b$^+$ Gr1^{high} MDSC (Fig. 3b).

Mechanism of T cell suppression by MDSC

To develop insights into the mechanism of MDSC-induced T cell suppression, we checked the expressions of CD40L, CD62L, CTLA-4 and PD-1 on T cells cultured without or with MDSC (Fig. 4a). The frequencies of T cells expressing CD40L were decreased and those expressing CTLA-4 were increased due to culture with MDSC ($n = 5$, $P < 0·05$) (Fig. 4b,c). However, the frequencies of CD62L and PD-1 were not altered significantly due to cultures with MDSC (Fig. 4b). The levels of expression of CTLA-4 and PD1 increased significantly on T cells due to culture with MDSC ($n = 5$, $P < 0·05$). In addition, the frequencies of

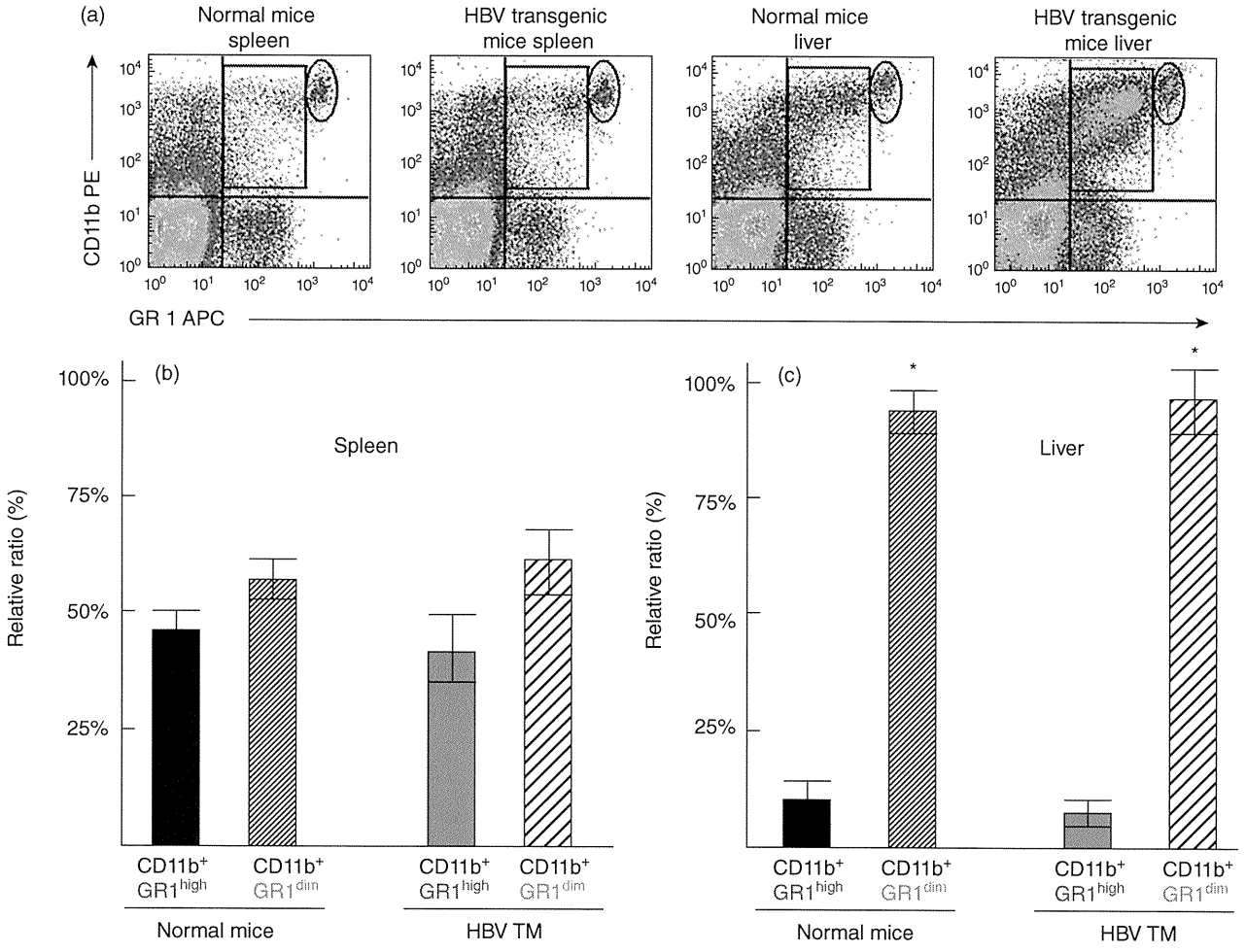

Fig. 1. Dual-colour flow cytometry shows myeloid-derived suppressor cells (MDSC) in the spleen and liver of normal mice and hepatitis B virus (HBV) transgenic mice (HBV TM) (a). MDSC in the upper right quadrant expressed both CD11b and Gr1 antigens. Depending on the expression of Gr1 antigen, two subtypes of MDSC were detected: one expressing high levels of Gr1 ($CD11b^+Gr1^{high}$) (shown by circle) and another expressing low levels of Gr1 ($CD11b^+Gr1^{dim}$) (shown by square). (b) Comparable frequencies of $CD11b^+Gr1^{high}$ MDSC and $CD11b^+Gr1^{dim}$ MDSC in the spleen of normal mice and HBV TM. (c) Significantly higher frequencies of $CD11b^+Gr1^{dim}$ MDSC compared to $CD11b^+Gr1^{high}$ MDSC in the liver of normal mice and HBV TM (c). * $P < 0{\cdot}05$, compared to $CD11b^+Gr1^{high}$ MDSC.

IFN-γ-producing T cells among total T cells were decreased significantly due to the addition of MDSC in T cell cultures compared to cultures without MDSC (1·81 ± 0·49% *versus* 6·11 ± 2·21%, respectively; $n = 5$, $P < 0{\cdot}05$) (Fig. 4d,e).

Immunosuppressive function of liver MDSC in a murine model of chronic HBV infection

To assess the immunosuppressive capacity of MDSC in chronic viral infection, we checked the frequencies and functions of MDSC in HBV TM, a murine model of chronic HBV carrier state [15]. The proportions of liver MDSC were significantly higher in HBV TM compared to normal mice (13·6 ± 3·2% *versus* 6·05 ± 1·21%, respectively; $P < 0{\cdot}05$, $n = 5$). In functional analyses, liver MDSC from HBV TM suppressed T cell proliferation in allogenic MLR in a dose-dependent manner (Fig. 5a).

To assess the role of MDSC on antigen-specific immune responses, lymphocytes from HBsAg-immunized normal C57BL/6J mice were stimulated by HBsAg without or with MDSC. As shown in Fig. 5b, MDSC from both normal mice and HBV TM suppressed proliferation of HBsAg-specific lymphocytes. Moreover, the levels of suppression were significantly higher in HBV TM-derived MDSC compared to normal mice-derived MDSC ($n = 5$, $P < 0{\cdot}05$) (Fig. 5b).

Discussion

Under physiological conditions, the liver maintains a state of immunological tolerance to various noxious substances to prevent extreme and detrimental immune reactions, although the liver harbours abundant amounts of immunocytes capable of inducing inflammation and cell damage. The immunosuppressive properties of the normal